48th AIAA Aerospace Sciences Meeting Including the New Horizons Forum and Aerospace Exposition
4 - 7 January 2010, Orlando, Florida
AIAA 2010-351

Detonation Turbulence Interaction

L. Massa, M. Chauhan and F. Lu

This paper reports a numerical study on the effect of turbulence on the detonation wave properties. The analysis is based on the integration of the chemically reactive Navier–Stokes equations using a Runge–Kutta scheme and a fifth-order WENO spatial discretization. We perform a direct numerical simulation (DNS) of the fluid-mechanics equations in three dimensions to determine the fine-scale evolution.

I. Introduction

The detonation–turbulence interaction problem is concerned with the unsteady coupling between convected vortical structures and a detonation wave. The dynamics of the interaction reveals the role of noise on detonation stability. A much more common type of interaction is the shock-turbulence coupling problem. Lee et al.[1] recently analyzed the coupling and found that the nonlinear problem agrees well with Ribner's linear interaction theory.[2] The detonation-turbulence interaction is different from the shock-turbulence interaction because of the role of the induction region in the amplification of convected vortical structures. Linear analysis[3] shows that the post-shock energy spectra are maximally amplified by the resonant interaction in the induction region. Linear analysis provides useful insights, but fails to correctly represent the system dynamics near natural frequencies.

Powers[4] discussed the modeling aspects of the multiscale case epitomized by a detonation wave along with results generated using single step kinetics for chemical reaction while emphasizing the necessity of capturing finer scales. A similar technique with one-step kinetics is used for the present work. The pre-shock turbulent field is incompressible, isotropic and chemically homogeneous. The post-shock field is strongly inhomogeneous because of the thermo-fluid coupling in the induction region. Ribner et al.[5] states that the effect of exothermicity is to amplify the rms fluctuations downstream of the detonation, with the greatest changes occurring around the Chapman-Jouguet Mach number with a restrictive assumption of the reaction zone thickness being much smaller than the turbulence length scale (but induction zones can be quite large). The influence of transverse waves on detonation and the pattern of quasi-steady detonation fronts are discussed by Dou et al.,.[6] The dynamics of small fluid-mechanics scales is vital to resolving the thermo-fluid interaction in the induction region of a detonation. An unstable detonation wave possesses a large set of intrinsic fluctuating frequencies with a range that increases with the activation energy.[3]

II. Governing equations

The governing equations are the nondimensional conservative form of the continuity, momentum and energy equations in Cartesian coordinates. The working fluid is assumed to be a perfect gas.

$$\frac{\partial \rho}{\partial t} + \frac{\partial}{\partial x_j}(\rho u_j) = 0 \tag{1a}$$

$$\frac{\partial}{\partial t}(\rho u_i) + \frac{\partial}{\partial x_j}(\rho u_i u_j + p\delta_{ij} - \sigma_{ij}) = 0, \quad i = 1, 2, 3 \tag{1b}$$

$$\frac{\partial E}{\partial t} + \frac{\partial}{\partial x_j}(E u_j + u_j p + q_j - u_i \sigma_{ij}) = 0 \tag{1c}$$

$$\frac{\partial \rho Z}{\partial t} + \frac{\partial}{\partial x_j}(\rho Z u_j) = (\rho - \rho Z) r(T) \tag{1d}$$

The non-dimensionalization is obtained using the equations given below, for the nonreactive terms,

$$\begin{aligned} x_i^* &= \frac{x_i}{L} \quad & t^* &= \frac{t}{L/V_\infty} \quad & \mu^* &= \frac{\mu}{\mu_\infty} \\ \rho^* &= \frac{\rho}{\rho_\infty} \quad & T^* &= \frac{T}{T_\infty} \quad & e^* &= \frac{e}{V_\infty^2} \\ u_i^* &= \frac{u_i}{V_\infty} \quad & p^* &= \frac{p}{\rho_\infty V_\infty^2} \end{aligned} \tag{2}$$

and for the reactive terms are obtained using the following relation

$$Q^* = \frac{Q\rho_\infty}{P_\infty} \quad E^* = \frac{E\rho_\infty}{P_\infty} \quad K_0^* = K_0 \frac{L}{V_\infty} \tag{3}$$

The variable Z is the reaction progress, where Z=0 describes the unburnt state and Z=1 the completely burnt state. The other variables are the same as in nonreactive case. Here, the total energy of the fluid is given by

$$E = \rho \left(\frac{P}{\gamma - 1} + \frac{u_i^2}{2} - QZ \right) \tag{4}$$

where Q is the heat release and the term $Q\rho Z$ denotes the chemical energy which is released as heat during the burning process. The reaction rate $r(T)$ is described by single step, Arrhenius law and depends on temperature T through the relation

$$r(T) = K_0 \exp^{-\left(\frac{E}{T}\right)} \tag{5}$$

where K_0 is the pre-exponential factor and it is also known as rate constant that sets the temporal scale of the reaction, E is the activation energy. The assumption of a single-step, Arrhenius kinetics law for $r(T)$ has been often employed in numerical studies. The important characteristics of the propagation of detonation waves can be sufficiently described by this simple chemistry model. On the other hand, this simplified model cannot provide an accurate description of the thermochemistry of real-life detonations and, therefore, its applicability has certain limitations.

III. Results

A. Computational set-up

A sketch of the computational set-up for the study of turbulence detonation interaction is shown in Fig. 1. The domain is three-dimensional with a square transversal section $(x - z)$ and periodic boundary conditions at the $x - y$ and $x - z$ planes. Non-reflective boundary conditions are implemented on the subsonic out-flow boundary. The conditions on the supersonic inflow are detailed in the following section.

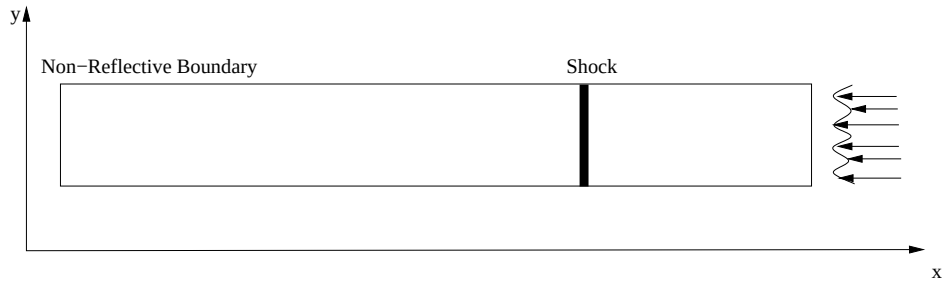

Figure 1. Sketch of the computational set-up.

B. Inflow boundary conditions

The inflow boundary conditions are implemented by imposing the fluid state on the supersonic inflow side. The procedure is similar to that described by Mahesh *et al.*[12] The flow is decomposed in a mean and perturbation part. The perturbation is evaluated by temporal decay of homogeneous compressible turbulence

in a cube with periodic boundary conditions. The initial spectrum is Gaussian and symmetric with spectral energy density

$$E = \frac{16\sqrt{\frac{2}{\pi}}\exp\left(-\frac{2k^2}{k_0^2}\right)k^4}{k_0^5}, \tag{6}$$

with $k_0 = 3$. The time-decayed turbulence is rescaled so that its length and velocity scales are the Taylor micro-scale λ and the velocity rms.

The shock-turbulence interaction is carried out by advecting the random field realization, thus assuming frozen dynamics. The conditions on the inflow boundary are thus spatially and temporally changing. The projection of the spectra for the three velocity components $u,\ v,\ w$ on the respective wave number components $k_x,\ k_y,\ k_z$ is shown in Fig. 2.

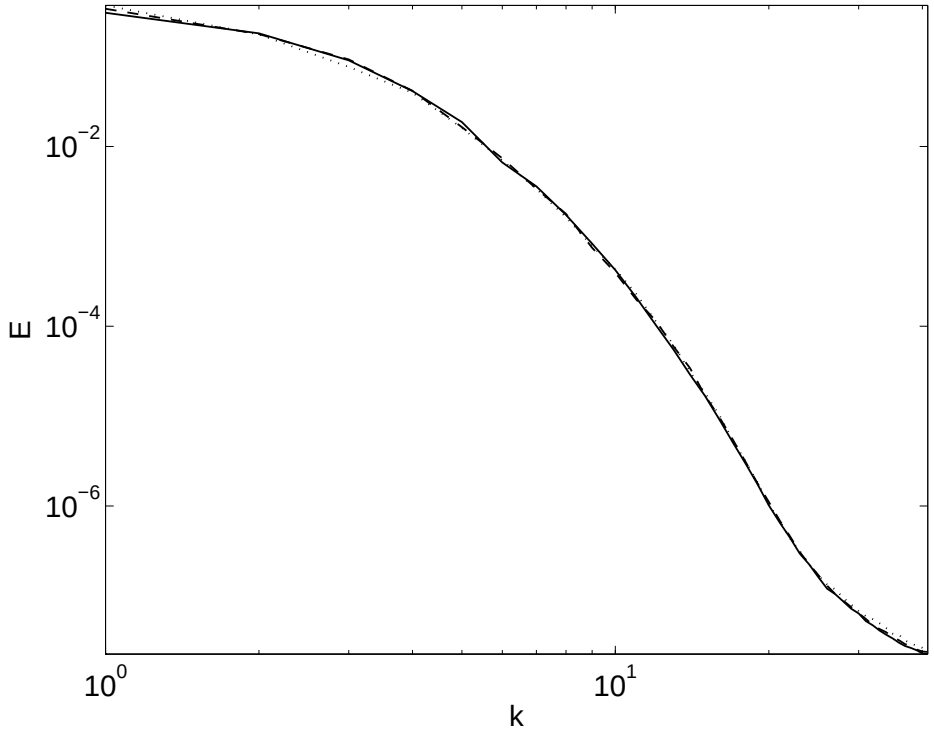

Figure 2. Initial spectrum. The three lines (solid, dashed and dotted) show the projections of the three-dimensional energy spectrum on the three wave number components $k_x,\ k_y,\ k_z$.

C. Computational grid

All computations were performed on $220 \times 80 \times 80$ grid with stretching in the direction perpendicular to the shock. The map from the computational to the physical space $\xi \to x$ is assigned in a polynomial form $x = \mathscr{P}(\xi)$ of order p. The computational domain extends $\xi \in [\xi_1, \xi_2]$, with $\xi_1 = 0$ and $\xi_2 = 13$ based on the Taylor micro-scale. The shock is located at $\xi_0 = 3/2\xi_2$. The conditions on the polynomial are

$$\mathscr{P}(\xi_1) = \xi_1 \qquad \mathscr{P}(\xi_2) = \xi_2,$$
$$\frac{\mathrm{d}\mathscr{P}}{\mathrm{d}\xi}(\xi_1) = 3 \qquad \frac{\mathrm{d}\mathscr{P}}{\mathrm{d}\xi}(\xi_1) = 2$$
$$\frac{\mathrm{d}\mathscr{P}}{\mathrm{d}\xi}(\xi_0) = 0.1 \qquad \frac{\mathrm{d}^k\mathscr{P}}{\mathrm{d}\xi^k}(\xi_0) = 0,\ k = 2, \ldots, p-5$$

D. Spectra

The focus on this paper is on the spatially varying spectral density and fluctuation intensity. By construction, the post-shock turbulent field is homogeneous in the $y-z$ directions and in time. One-dimensional power spectra are built upon time sequences. The time replaces the longitudinal pre-shock wave number considered by Ribner[2] by virtue of the assumption assumption of frozen perturbation dynamics in the pre-shock field. In the linear regime the pre-shock vortical field can be decomposed in the superposition of planar waves[2] and the temporal and longitudinal frequencies scale according to $k_t/k_1 = D_s$.

A scalar field $\alpha(\vec{x},t)$ is expanded over the (x_2, x_3, t) space in Fourier-Stieltjes series in the general form

$$\alpha(\vec{x},t) = \int e^{i[k_2,k_3,k_t]^T[x_2,x_3,t]}\,\mathrm{d}Z_\alpha(k_2,k_3,k_t,x_1), \tag{7}$$

where k_2 and k_3 are the wave number vector projections onto the respective Cartesian axes. The one dimensional power spectrum for the variable α is defined as

$$\Phi_\alpha(k_t) = \iint [\alpha\alpha](k_2,k_3,k_t,x_1)\,\overline{u^2}_\infty\,\mathrm{d}\hat{k}_2\,\mathrm{d}\hat{k}_3, \tag{8}$$

where $\overline{u^2}_\infty$ is the pre-shock longitudinal velocity variance. Numerically, the spectral density $[\alpha\alpha] \equiv |\,\mathrm{d}Z_\alpha|^2$ is determined by applying discrete Fourier transforms (DFT) to the random fields, and the integral are replaced by summations. In the discrete analog of equation (8) the discrete Parseval relation is maintained, meaning that the field variance $\overline{\alpha^2}_0$ is equal to the mean of the discrete spectra.

Spectra and variances are evaluated by determining flow statistics over an interval of $\Delta t = 1$. This time interval is non-dimensionalized using the Taylor micro-scale and the longitudinal velocity rms.

E. Comparison between reactive and non-reactive cases

The comparison between reactive (detonation-turbulence interaction) and non-reactive (shock-turbulence interaction) simulation is performed maintaining the same Mach number M_∞ and ratio of specific heat $\gamma = 1.2$, while setting the overdrive $f = 1$ and the activation energy $E = 20$ in the reactive simulation. The heat release parameter is determined as,

$$\frac{Q\rho_\infty}{p_\infty} = \frac{\gamma\left(f^2 - 2fM_\infty^2 + M_\infty^4\right)}{2f\left(\gamma^2-1\right)M_\infty^2},$$

which for $f = 1$ (Chapman-Joguet) detonation simplifies to,

$$\frac{Q\rho_\infty}{p_\infty} = \frac{\gamma\left(M_\infty^2-1\right)^2}{2\left(\gamma^2-1\right)M_\infty^2}. \tag{9}$$

For all calculations presented here, the ratio between Taylor micro-scale and reaction half distance was kept constant and unitary, $\mathscr{N} \equiv \lambda/l_{1/2} = 1$. Note, all calculations are in the shock reference frame, thus $M_\infty > 1$ is the detonation Mach number.

F. Low heat release

The first comparison is performed for $M_\infty = 1.75$, which implies that $Q = 1.89413$. The pressure and velocity profiles for this detonation are shown in Fig. 3. The linear interaction analysis[3] shows that the response of the waves to pre-shock turbulent forcing is closely related to its normal modes. A stability analysis for this detonation wave reveals the presence of on unstable mode. The normal mode dispersion relation for this structure is shown in Figs. 4 and 5. In this figure the values of k and α are expressed in units of $\sqrt{p_\infty/\rho_\infty}$ and $l_{1/2}$ (half reaction distance), to set them independently of the pre-shock turbulent field.

1. Velocity variances

Because of the variation of the mean-flow with x, fluctuations are evaluated about a space-dependent mean. The mean is taken equivalent to the one-dimensional profile shown in Fig. 3. Only the post-shock field is presently considered. The velocity variances are plotted against the distance from the shock in Fig. 6. Both

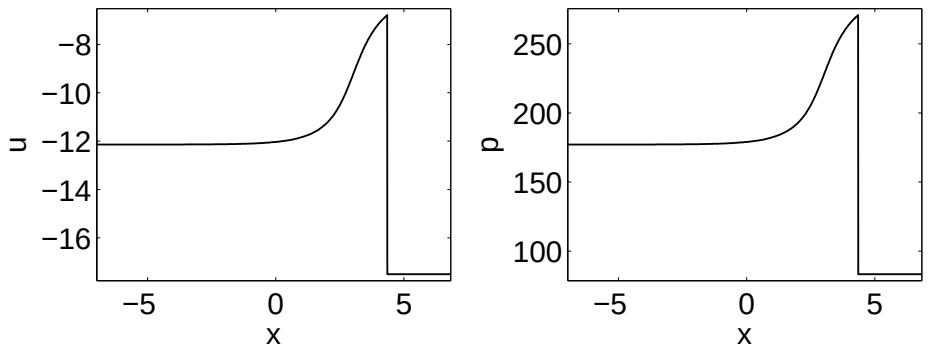

Figure 3. Detonation structure. Velocity and pressure versus normal distance x. Note: detonation reference frame.

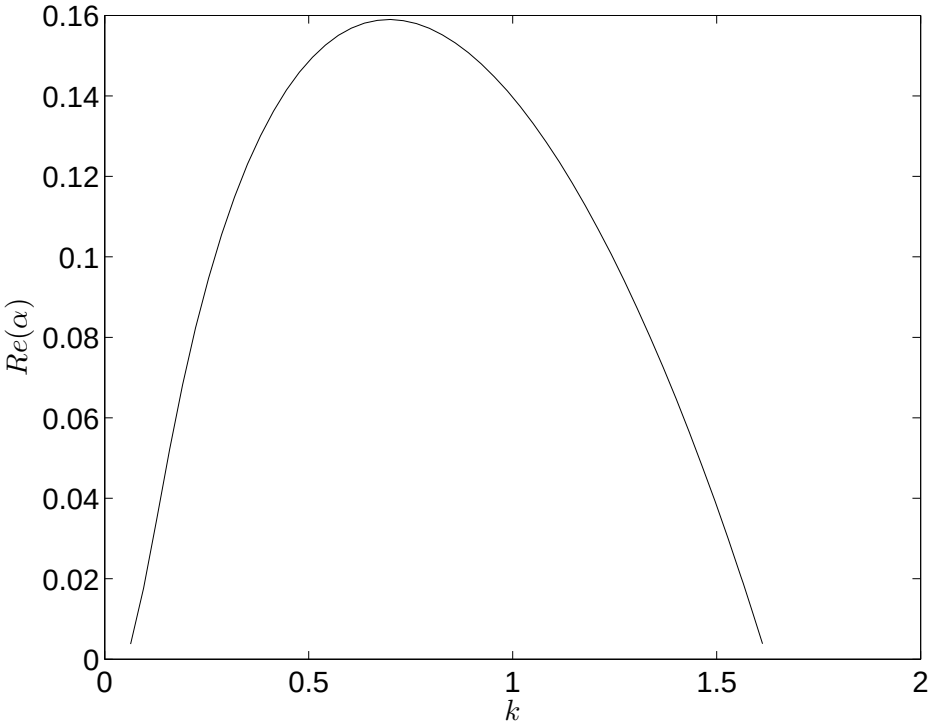

Figure 4. Normal mode dispersion relation for low heat release detonation. Real part of the growth rate eigenvalue.

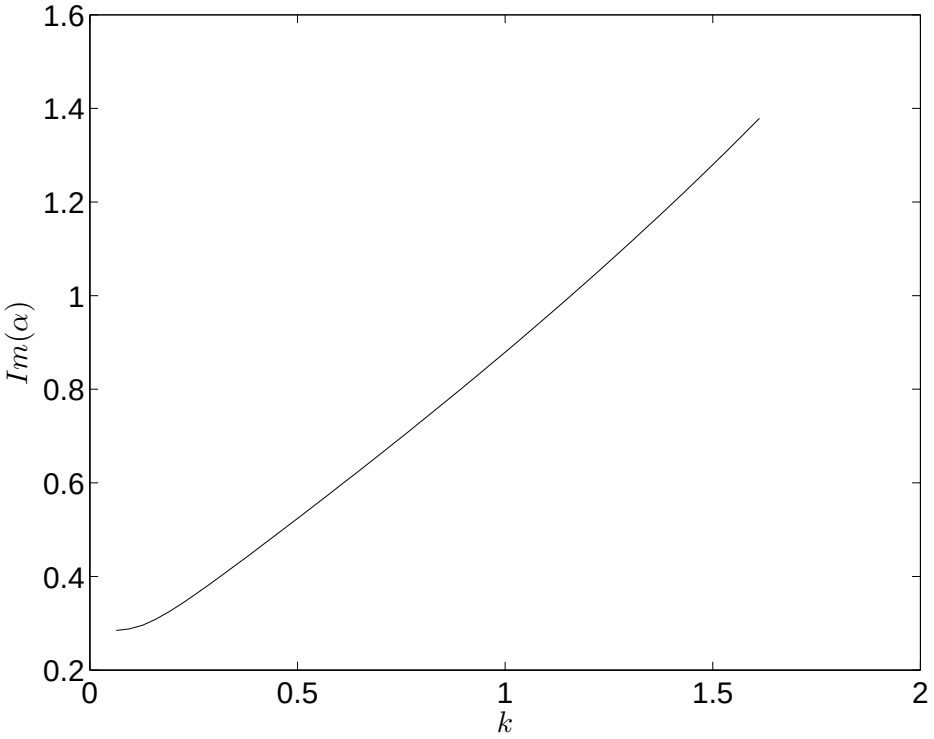

Figure 5. Normal mode dispersion relation for low heat release detonation. Imaginary part of the growth rate eigenvalue.

the v and w components are plotted to verify that the flow is isotropic in planes parallel to the shock front. The plots show that the fluctuation intensities are not significantly affected by the addition of the heat release. The reactive solution (right panel in Fig. 6) manifests a slower increase of the longitudinal velocity variance in the post-shock region.

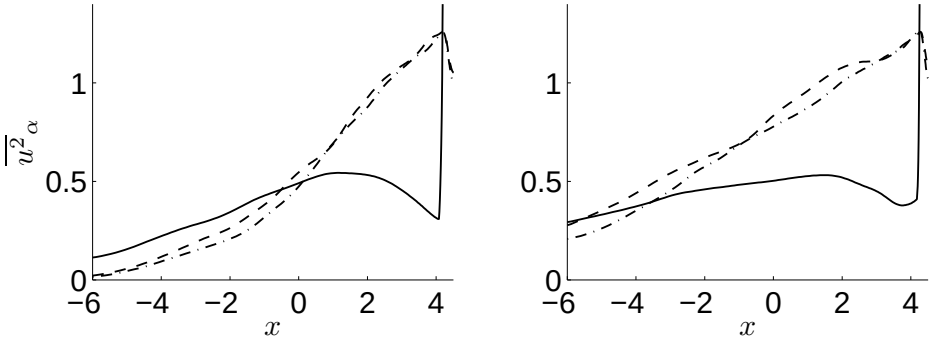

Figure 6. Longitudinal velocity variance as a function of the distance. The left panel is the non-reactive solution, the right panel is the reactive counterpart.

G. Medium heat release

The case under consideration is characterized by a detonation/shock Mach number $M_\infty = 4$. According to equation (9) the heat release parameter is $Q\rho_\infty/p_\infty = 19.176$. The resulting detonation has three unstable normal modes. The dispersion relation $\alpha\,(k)$ is shown in Figs. 7 and 8. Similarly as in Fig. 4, the velocity scale is based on pre-shock pressure and density rather than on the longitudinal velocity rms. Thus, in order

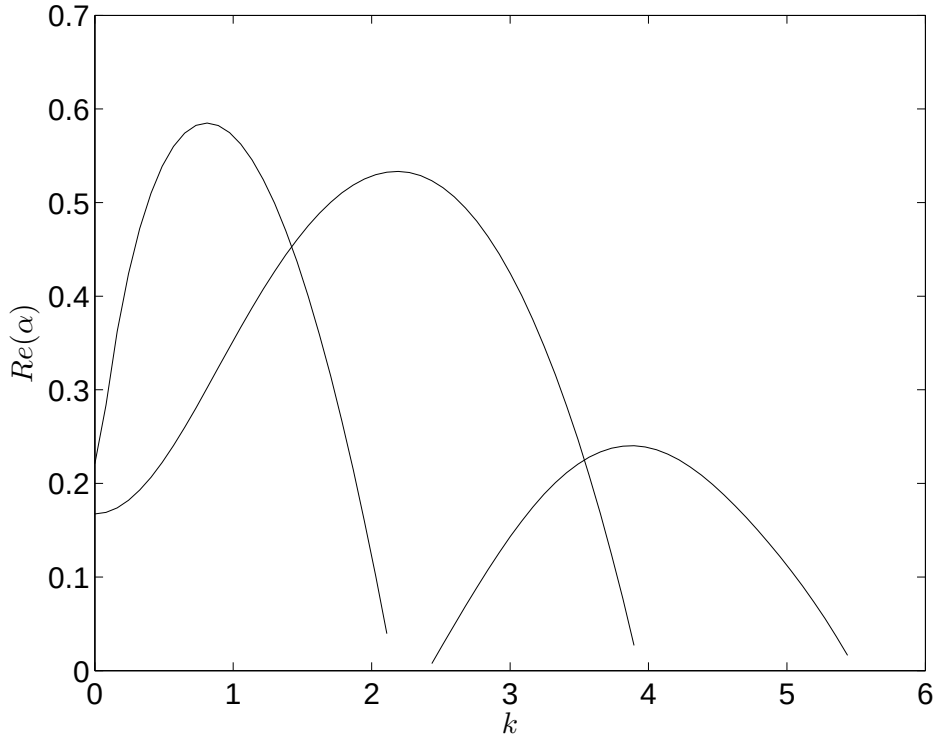

Figure 7. Normal mode dispersion relation for medium heat release detonation: real part of the growth rate.

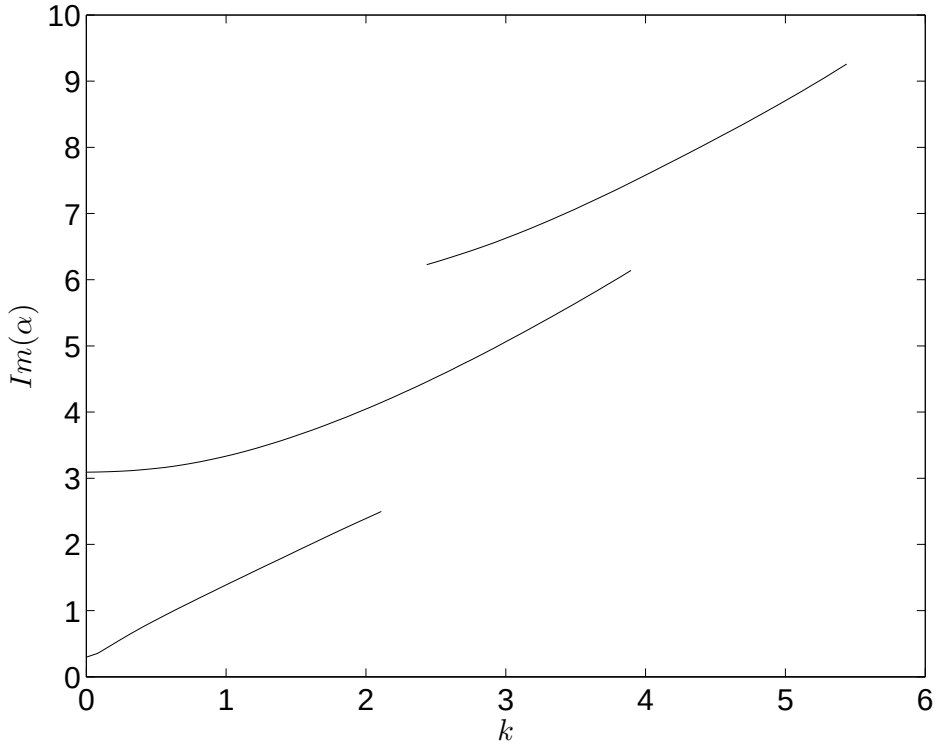

Figure 8. Normal mode dispersion relation for medium heat release detonation, imaginary part of the growth rate.

to compare the results in Figs. 7 and 8 to the three dimensional simulations the y-axis must be scaled by $1/\left(\sqrt{\gamma}M_t\right)$.

Note that the detonation is longitudinally unstable. In the linear stability analysis the perturbation of the shock front has the form $\psi = \exp\left(\alpha t + ky\right)$, thus variations of the mean shock location require $\alpha\left(k=0\right) \neq 0$. Longitudinal instability leads to a limit cycle in the form of a galloping wave, for which the mean shock location is periodic in time. For this reason the perturbation is evaluated about a time/x dependent spatial (y-z) average, rather than the x dependent mean profile used for the previous case.

For the present case the turbulent Mach number M_t was reduced to 0.05 due to the large shock front deformation occurring in both the reactive and non-reactive cases. The simulation interval was $T = 2$, and statistics were collect on $t \in [1, 2]$. The longitudinal velocity is visualized on nine $x - z$ cuts in Figs. 9 and 10 for a time representative of the unsteady evolution. In the non-reactive simulation the shock front impinges

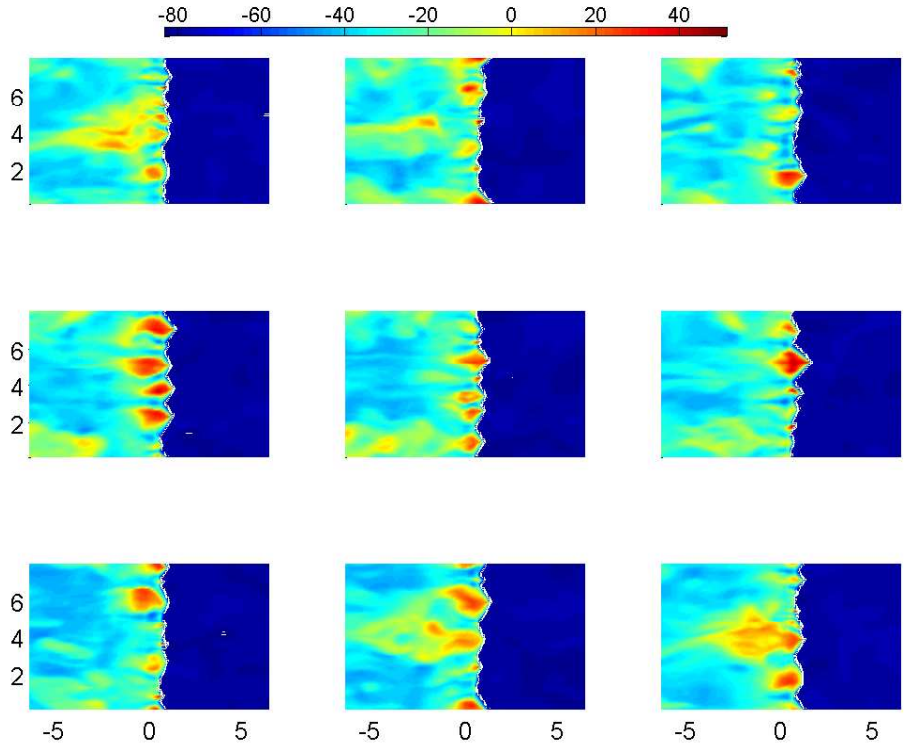

Figure 9. Longitudinal velocity in reactive $M = 4$ case: $x - z$ cuts.

on the inflow boundary (see the right hand side of all panels in Fig. 10). This phenomenon is accentuated by an increase in turbulent Mach number, and is the rationale that lead to the reduction of M_t with respect to the value used in the low heat release simulations.

1. Velocity variances

The intrinsic instability of the detonation wave (see Fig. 7) makes the process intrinsically unsteady, thus unforced detonations (i.e., zero incoming turbulence) perform limit cycle oscillations. Therefore, in the reactive case, the post-shock perturbation is composed by a natural spectrum (i.e., independent of the forcing) and a response to the turbulent inflow. In order to determine both contributions, variances are presented for three case: i) the reactive case with incoming Gaussian turbulence, ii) non-reactive case with incoming Gaussian turbulence, and iii) reactive case with non-perturbed (zero turbulence) free-stream.

The variances are determined as space-temporal means about the $y - z$ averages. The zero x (0_x) of the reference frame is fixed with the shock location, which, due to the longitudinal instability, moves with respect to the mean detonation velocity $M_\infty\sqrt{\gamma p_\infty/\rho_\infty}$. The 0_x corresponds with the maximum value of the

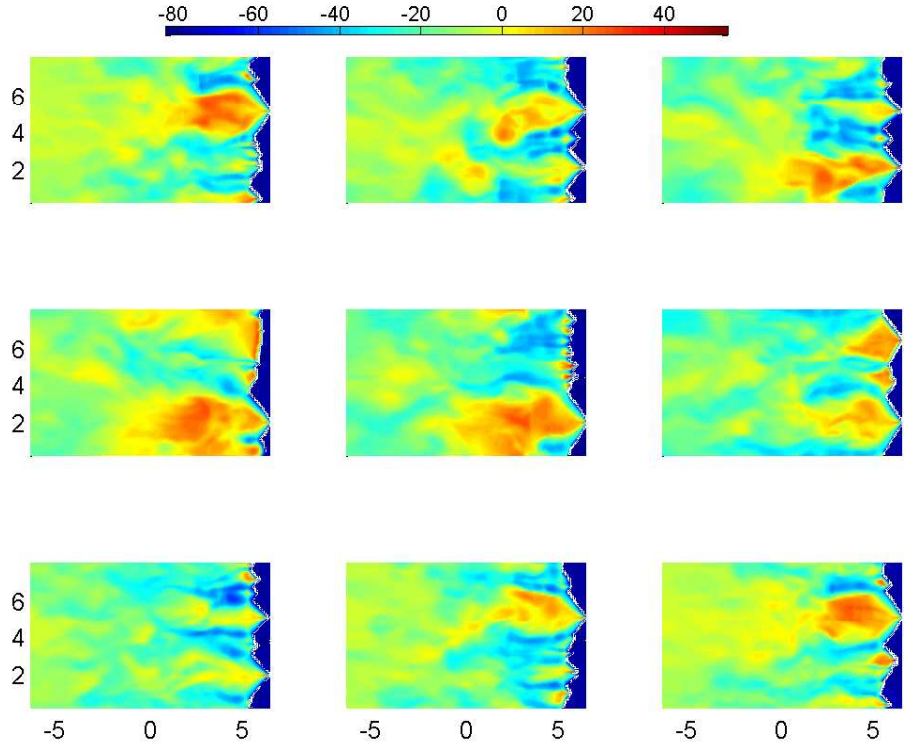

Figure 10. Longitudinal velocity in non-reactive $M = 4$ case: $x - z$ cuts.

derivative of the $y-z$ mean of the pressure, $\frac{\partial \overline{(p)}_{yz}}{\partial x}$. Note that for the non-reactive case the shock location is approximately constant in the mean shock frame.

The longitudinal perturbation variances for the three cases are shown in Fig. 11, where the solid, dashed and dotted lines are used for reactive, non-reactive and non-perturbed cases respectively. The results in

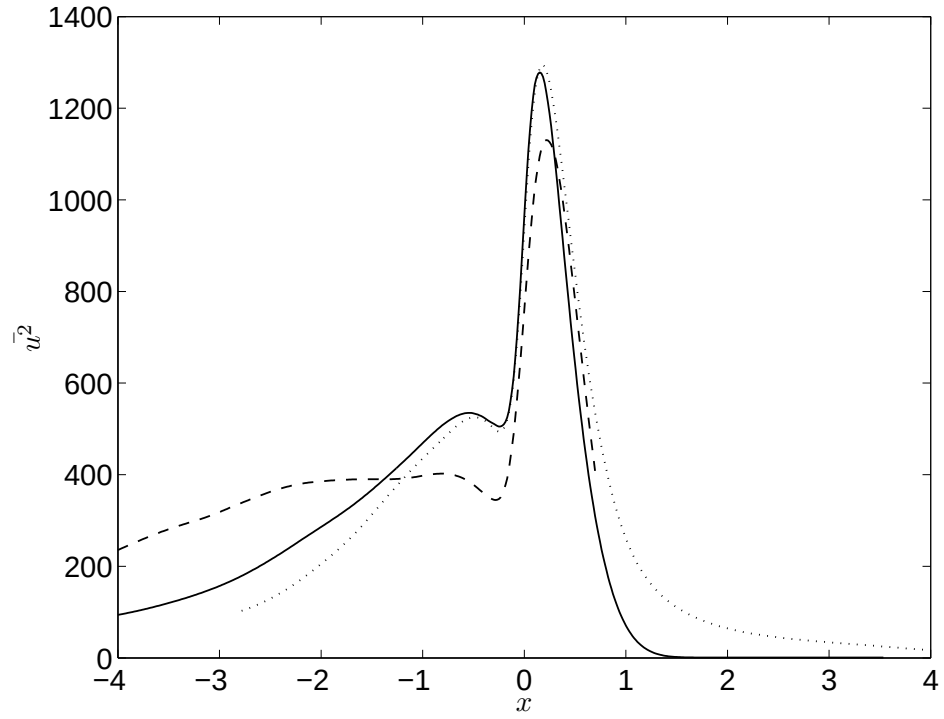

Figure 11. Longitudinal velocity variance against distance from the shock. Solid, dashed and dotted lines are used for reactive, non-reactive and non-perturbed cases respectively.

Fig. 11 support the conclusion that adding a free-stream perturbation leads to an increased longitudinal velocity variance behind an unstable detonation, and that reactivity leads to an increase in the same quantity. Nonetheless, the turbulent field behind the detonation appears to be dominated by the natural spectrum, the one generated by the intrinsic instability.

2. Power spectra

The power spectra for longitudinal velocity are displayed in Fig. 12 at nine distances from the shock, as indicated on top of each panel. In all plots the solid line refers to the reactive, the dashed to the non-reactive solution and the dash-dot line to the unforced solution. The x coordinate is measured from the shock plane. Peaks can be observed in the last two panels ($x = 1.5$ and $x = 2$), which are similar to the characteristic peaks noted in the linear analysis.[3] Note that neutral frequencies for $M_t = 0.05$ and $\gamma = 1.2$ are from Fig. 8 $\alpha_n = [45.582, 112.08, 169.03]^T$.

References

[1]Lee, S., Lele, S.K. and Moin, P., "Interaction of Isotropic Turbulence with Shock Waves: Effect of Shock Strength. *Journal of Fluid Mechanics*, Vol. 340, pp. 225-247, 1997.

[2]Ribner, H.S., "Spectra of Noise and Amplified Turbulence Emanating from Shock-Turbulence Interaction," *AIAA Journal*, Vol. 25, No. 3), pp. 436–442, 1987.

[3]Massa, L. and Lu, F.K., "Role of the induction zone on turbulence-detonation interaction," AIAA-2009.

[4]Powers, J.D., "Review of Multiscale Modeling of Detonation," *Journal of Propulsion and Power*, Vol. 22, No. 6, pp. 1217–1229, 2006.

[5]Jackson, T.L., Hussaini, M.Y. and Ribner, H.S., "Interaction of Turbulence with a Detonation W ave," *Physics of Fluids A*, Vol. 5, No. 3, pp. 745–749, 1993.

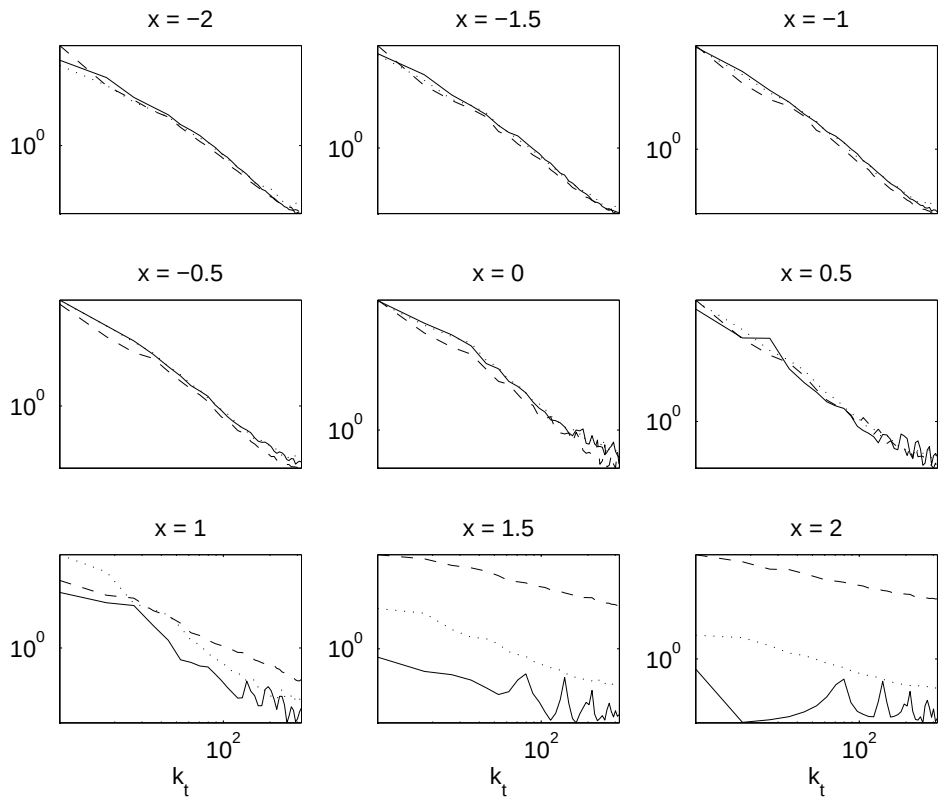

Figure 12. Longitudinal velocity power spectrum at four distances from the shock. Solid, dashed and dotted lines are used for reactive, non-reactive and non-perturbed cases respectively.

[6]Dou, H.-S., Tsai, H.M., Khoo, B.C. and Qiu, J., "Simulations of Detonation Wave Propagation in Rectangular Ducts Using a Three-Dimensional WENO Scheme," *Combustion and Flame*, Vol. 154, No. 4, pp. 644–659, 2008.

[7]Arakawa, A., "Computational Design for Long-Term Numerical Integration of the Equations of Fluid Motion. Part I," *Journal of Computational Physics*, Vol. 1, No. 1, pp. 119–143, 1966.

[8]Mansour, N.N. and Wray, A.A., "Decay of Isotropic Turbulence at Low Reynolds Number," *Physics of Fluids*, Vol. 6, No. 2, pp. 808–814, 1994.

[9]Rogallo, R.S., "Numerical Experiments in Homogeneouos Turbulence," NASA TM-81315, 1981.

[10]Mohseni, K., Kosović, B., Shkoller, S., Marsden, E.J., "Numerical Simulations of the Lagrangian Averaged Navier-Stokes Equations for Homogeneous Isotropic Turbulence," *Physics of Fluids*, Vol. 15, No. 2, pp. 524–544, 2003.

[11]Meneveau, C., Lund, T.S., "On the Lagrangian Nature of the Turbulence Energy Cascade," *Physics of Fluids*, Vol. 6, No. 8, pp. 2820–2825 , 1994.

[12]K. Mahesh, S.K. Lele, and P Moin, "The influence of entropy fluctuations on the interaction of turbulence with a shock wave," *Journal of Fluid Mech.*, Vol. 334, pp. 353–379, 1997.